BILINGUAL PUBLISHING CO.
Pioneer of Global Academics Since 1984

Journal of Architectural Environment & Structural Engineering Research
https://ojs.bilpublishing.com/index.php/jaeser

ARTICLE

Structural Performance of Smart CFRP-FBG Reinforced Steel Beams

Huaping Wang[1,2*] Tao Song[1] Hengyang Li[1] Siyuan Feng[1]

1. School of Civil Engineering and Mechanics, Lanzhou University, Lanzhou, Gansu, 730000, China
2. Key Lab of Structures Dynamic Behavior and Control (Harbin Institute of Technology), Ministry of Education, Harbin, Heilongjiang, 150090, China

ARTICLE INFO

Article history
Received: 22 June 2020
Accepted: 14 August 2020
Published Online: 31 October 2020

Keywords:
CFRP reinforced beam
Interfacial interaction
Smart CFRP-FBG plate
Deflection
Experimental investigation

ABSTRACT

Many beam structures suffer from gradual performance degradation with the increase of service life. To recover the bearing capacity of these beams, carbon fiber reinforced polymer (CFRP) plates are developed to attached on the beam bottom. To check the structural performance of the CFRP reinforced beams, smart CFRP plate with FBGs in series is designed and LVDTs are adopted to measure the deformations. The deflection of the reinforced beam is given based on the elastic conversion cross-section method. The experimental results validate the effectiveness of the proposed algorithm. The study shows that the CFRP reinforced zone has a larger flexural rigidity than the pure steel beam zone. The general distribution of the deflection along the span of the CFRP reinforced beam can be described by the proposed formula. It provides a scientific design guidance for the deflection control of CFRP reinforced structures.

1. Introduction

A great number of built structures all over the world are stepping into aging stages. For steel beam structures, fatigue damage is responsible for the major failure mode. To extend the service life of these aging steel structures, retrofit measures are usually proposed. Carbon fiber reinforced polymer (CFRP) composites have been proposed for the main choice for the excellent advantages of high strength-to-weight ratio and stiffness, corrosion resistance, good durability and fatigue performance and light weight. Using the externally bonded CFRP composites on the tensile surface of steel beam structures to strengthen the structures has attracted increasing attention [1-3]. Considerable study shows that the flexural and shear performance and load-carrying capacity of the reinforced structures can be improved. However, the design method, damage and failure mechanisms, and durability of CFRP reinforced structures are yet to be fully investigated.

The interfacial bonding quality between the CFRP plate and the substrate layer is of considerable concern. The long-term performance of CFRP-to-steel bonded layer can be affected by special ambient environmental conditions (i.e., the high or sub-zero temperature, humidity, seawater, static and dynamic loading modes). The retrofit efficiency can be finally attributed to the performance of the bonding adhesive. Debonding damage is the major concern for the safety of CFRP plate reinforced structures [4-5]. European

**Corresponding Author:*
Huaping Wang,
School of Civil Engineering and Mechanics, Lanzhou University, Lanzhou, Gansu, 730000, China;
Key Lab of Structures Dynamic Behavior and Control (Harbin Institute of Technology), Ministry of Education, Harbin, Heilongjiang, 150090, China;
Email: wanghuaping1128@sina.cn; hpwang@lzu.edu.cn

 DOI: https://doi.org/10.30564/jaeser.v3i4.2035

studies indicate that compared with strength control, the deflection control is the most significant for the design of CFRP reinforced bridges. To make full use of the CFRP reinforced structures, the deformation resistance should be improved, which means that the flexural rigidity should be enhanced.

Attempts have been conducted to understand the mechanical behavior of CFRP strengthened steel structures by experimental studies, numerical analysis and theoretical exploration. To judge the effectiveness of the proposed strengthen measure, optical fiber sensing technology is adopted to monitor the real-time and long-term performance of the CFRP reinforced structures. The outstanding advantages of optical fiber sensing technique over the ultrasonic imaging, eddy current method, thermography and wave method focus on the stable whole-process detection with low cost and high accuracy [6-8]. Smart CFRP plate is thus developed, with FBGs in series embedded to measure the normal strain of the CFRP plate during the service period [9-13]. Based on the theoretical study in Ref. [14], the interfacial shear stress can be obtained, which can be adopted to judge the interfacial performance of the reinforced structures.

In this paper, the interfacial interaction of the smart CFRP-FBG composites reinforced steel beams is discussed based on the preliminary study. The interfacial shear stress and normal stress of the CFRP plate along the span of the reinforced beam are displayed. The deflection along the span of the CFRP reinforced beam is also proposed based on the elastic conversion cross-section method. The comparison study on the calculated deflection and the measured deflection with LVDTs is further performed to check the feasibility and effectiveness of the proposed algorithm.

2. Stress State of the CFRP Reinforced Steel Beam

To monitor the interfacial debonding of a CFRP reinforced structure, it is essential to understand the mutual interaction and the damage mechanism. Therefore, a theoretical model is first formulated to describe the stress relationships. A steel beam model with a H-shaped cross section is considered, where a CFRP composite is attached on the beam bottom. As shown in Figure 1, the simply supported constraint and four-point bending loading are considered. The span and the height of the beam are $2(l+a)$ and $2z_0$, respectively. The length, width and thickness of the CFRP composite are separately denoted as $2l$, b_c and t_c. The origin of the coordinate system is located at the neutral axis of the beam, as shown in Figure 1. P is the load, and b is the distance of the load point to the origin of the coordinate.

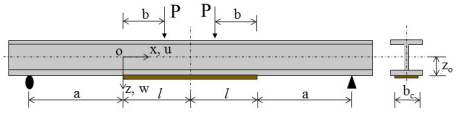

Figure 1. Steel beam strengthened with CFRP composite

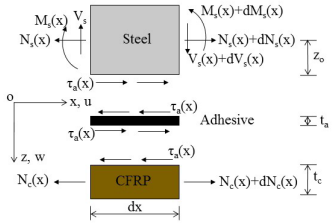

Figure 2. Infinitesimal element of a three-layered strengthened beam

An arbitrary cross section is considered in the theoretical derivation. An infinitesimal element, dx, is selected from the CFRP reinforced beam. The stress state of a three-layered model is shown in Figure 2. $M_s(x)$, $N_s(x)$ and $V_s(x)$ are the bending moment, axial force and shear force of the steel beam, respectively. $N_c(x)$ is the axial force of the CFRP plate. $\tau_a(x)$ is the interfacial shear stress. The thickness of the adhesive layer is t_a. Two assumptions are made: (1) the bending stiffness of the beam to be strengthened is much greater than the stiffness of the strengthening plate; and (2) the stresses in the adhesive layer don't change along the thickness direction (i.e., the adhesive layer is thin). Therefore, the bending moment in the CFRP composite is negligible, which implies that the normal stress in the bonding zone can be ignored, as displayed in Figure 2.

The interfacial shear stress can be obtained from the reference [15]. If $\lambda b > 5$, it gives

$$\tau_a(x) = \frac{G_a P}{t_a E_s W_s} \frac{a\lambda e^{-\lambda x} + 1}{\lambda^2} \tag{1}$$

where $\lambda^2 = \frac{G_a b_c}{t_a}\left(\frac{1}{E_c A_c} + \frac{z_o}{E_s W_s} + \frac{1}{E_s A_s}\right)$, and the normal stress of the CFRP composite can be expressed as

$$\sigma_c(x) = \frac{G_a P}{t_c t_a E_s W_s} \frac{a(1-e^{-\lambda x}) + x}{\lambda^2},\ 0 \le x \le b \tag{2}$$

The geometrical and material parameters of the steel beam and the CFRP composite are described in Table 1. The parameters a, b and l are 550 mm, 200 mm and 350

DOI: https://doi.org/10.30564/jaeser.v3i4.2035

mm, respectively. Substituting correlated parameters in Table 1 into the formula of λ, the value λ*b* can be figured out, with value 6. 76 larger than 5. Therefore, the proposed Eq. (1) and Eq. (2) can be adopted to describe the interfacial action of the model. The profiles of the interfacial shear stress and the normal stress of the CFRP composite under the different loads (*P* = 1kN, 10 kN, 20 kN, 30 kN) can be obtained by substituting the given parameters into Eq. (1) and Eq. (2). The abscissa axis in Figure 3 is *x*, with its value ranging from 0 to *b*. It can be noted that the interfacial shear stress decreases nonlinearly from the end to the central, with the maximum value in the end (*x*=0) in Figure 3(a). The normal stress of the CFRP composite presents an increasing tendency from the end to the central, and the maximum value occurs in the central in Figure 3(b). The normal stresses of the CFRP plate are generally far larger than the interfacial shear stress. The interfacial shear stress decreases from the end of the CFRP plate to the central, with maximum value at the end.

Table 1. Physical parameters of the CFRP reinforced steel beam in test

Content	Label	Value	Unit
Flange thickness of steel beam		9×10^{-3}	m
Web width of steel beam		6×10^{-3}	m
Width of steel beam		1.25×10^{-1}	m
Half of the height of steel beam	z_0	6.25×10^{-2}	m
Area of cross section of steel beam	A_s	2.892×10^{-3}	m^2
Area of cross section of CFRP plate	A_c	3×10^{-4}	m^2
Width of CFRP plate	b_c	1×10^{-1}	m
Thickness of CFRP plate	t_c	3×10^{-3}	m
Thickness of adhesive layer	t_a	1.5×10^{-3}	m
Young's modulus of steel	E_s	2.06×10^{11}	N/m^2
Young's modulus of CFRP	E_c	3.07×10^{11}	N/m^2
Shear modulus of adhesive layer	G_a	1.154×10^{9}	N/m^2

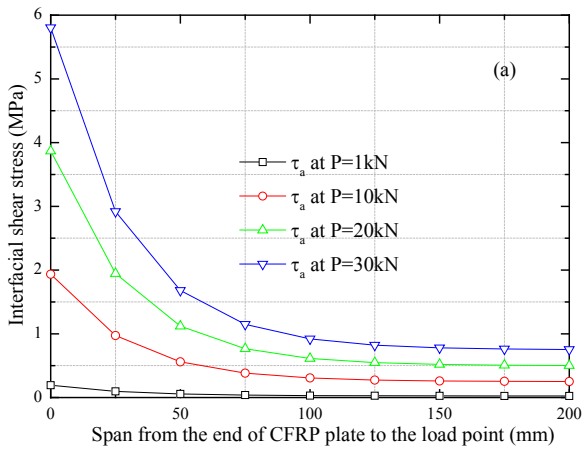

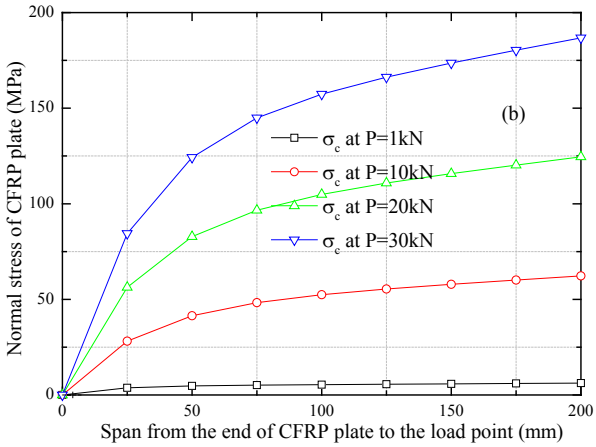

Figure 3. Profiles of (a) the interfacial shear stress and (b) the normal stress of CFRP plate

3. Deflection of the CFRP Reinforced Steel Beam

For the CFRP reinforced beam under the four-point bending load as shown in Figure 4, the bending moments at different sections can be described as

$$M(x) = Px \qquad (0 \le x \le a) \tag{3a}$$

$$M(x) = Px \qquad (a \le x \le b) \tag{3b}$$

$$M(x) = P(a+b) \qquad (b \le x \le a+l) \tag{3c}$$

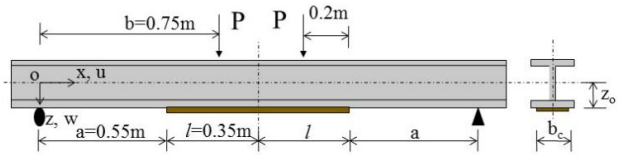

Figure 4. The geometrical size of the CFRP reinforced steel beam

In the interval [0, *a*], the approporiate relationship of the deflection and the bending moment of the steel beam in the coordinate system as displayed in Figure 4 can be given by

$$\frac{d^2 f(x)}{dx^2} = -\frac{M(x)}{EI} \tag{4}$$

where *M(x)* is respect to *x* ranged from 0 to *a*, and *E* and *I* are the elastic modulus and the cross-section moment of inertia of the H-steel beam. Substituting Eq.(3a) into Eq.(4), the following formula can be obtained:

DOI: https://doi.org/10.30564/jaeser.v3i4.2035

$$\frac{d^2 f(x)}{dx^2} = -\frac{Px}{E_s I_s} \tag{5}$$

Taking the quadratic integral of Eq.(5) with respect to x, the deflection can be expressed as

$$f(x) = -(\frac{Px^3}{6E_s I_s} + C_1 x + C_2) \qquad 0 \le x \le a \tag{6}$$

where $C_1$and C_2 are constant coefficients and can be determined by boundary conditions.

In the interval [*a, b*], the elastic conversion cross-section method can be adopted to explain the relationship of the deflection and the bending moment of the CFRP reinforced beam:

$$\frac{d^2 f(x)}{dx^2} = -\frac{M(x)}{E_s I_{eq}} \tag{7}$$

where the equivalent cross-section moment of inertia $I_{eq} = I_0 + A_0 d_c^2$, $I_0 = I_s + I_c / \alpha_E$, $A_0 = A_s A_c / (\alpha_E A_s + A_c)$, $\alpha_E = E_s / E_c$, d_c is the distance between the cores of the steel beam and the smart CFRP plate.

Substituting Eq.(3b) into Eq.(7) and taking the quadratic integral, the expression of the deflection can be given:

$$f(x) = -(\frac{Px^3}{6E_s I_{eq}} + C_3 x + C_4) \qquad a \le x \le b \tag{8}$$

where C_3 and C_4 are constant coefficients and can be determined by boundary conditions.

In the interval [*b, a*+l], the deflection can be obtained in the similar way:

$$f(x) = -(\frac{P(a+b)}{2E_s I_{eq}} x^2 + C_5 x + C_6) \qquad b \le x \le a+l \tag{9}$$

where C_5 and C_6 are constant coefficients and can be determined by boundary conditions. The midspan deflection reaches the maximum value, and then its first derivative is 0, which thus gives $\frac{df(x)}{dx} = [\frac{P(a+b)}{E_s I_{eq}} x + C_5]\big|_{x=a+l} = 0$ and $C_5 = -\frac{P(a+b)(a+l)}{E_s I_{eq}}$. Eq.(9) can thus be expressed as

$$f(x) = -[\frac{P(a+b)}{2E_s I_{eq}} x^2 - \frac{P(a+b)(a+l)}{E_s I_{eq}} x + C_6] \qquad b \le x \le a+l \tag{10}$$

Since the deflection at the left support is 0, it yields $f(x)\big|_{x=0} = 0$ and C_2=0. Thus, Eq.(6) can be rewritten as

$$f(x) = -(\frac{Px^3}{6E_s I_s} + C_1 x) \qquad 0 \le x \le a \tag{11}$$

According to the continuous conditions, the deflections and the angles at point a should be equal to that at point b, which gives:

$$f(a) = \frac{Pa^3}{6E_s I_s} + C_1 a = \frac{Pa^3}{6E_s I_{eq}} + C_3 a + C_4 \tag{12a}$$

$$\frac{df(x)}{dx}\Big|_{x=a} = \frac{Pa^2}{2E_s I_s} + C_1 = \frac{Pa^2}{2E_s I_{eq}} + C_3 \tag{12b}$$

$$f(b) = \frac{Pb^3}{6E_s I_{eq}} + C_3 b + C_4 = \frac{P(a+b)}{2E_s I_{eq}} b^2 - \frac{P(a+b)(a+l)}{E_s I_{eq}} b + C_6 \tag{12c}$$

$$\frac{df(x)}{dx}\Big|_{x=b} = \frac{Pb^2}{2E_s I_{eq}} + C_3 = \frac{P(a+b)}{E_s I_{eq}} b - \frac{P(a+b)(a+l)}{E_s I_{eq}} \tag{12d}$$

and then the constants can be figured out:

$$C_3 = \frac{P}{E_s I_{eq}}(\frac{b^2}{2} - a^2 - al - lb),$$

$$C_1 = \frac{P}{E_s I_{eq}}(\frac{b^2 - a^2}{2} - al - lb) - \frac{Pa^2}{2E_s I_s},$$

$$C_4 = \frac{Pa^3}{3E_s I_{eq}} - \frac{Pa^3}{3E_s I_s},$$

$$C_6 = \frac{Pb^3}{6E_s I_{eq}} + \frac{Pab^2}{2E_s I_{eq}} + \frac{Pa^3}{3E_s I_{eq}} - \frac{Pa^3}{3E_s I_s}$$

Substituting these parameters into Eq.(8), Eq.(10) and Eq.(11), the deflections at different intervals can be expressed as

$$f(x) = -\{\frac{Px^3}{6E_s I_s} + [\frac{P}{E_s I_{eq}}(\frac{b^2 - a^2}{2} - al - lb) - \frac{Pa^2}{2E_s I_s}]x\} \qquad 0 \le x \le a \tag{13a}$$

DOI: https://doi.org/10.30564/jaeser.v3i4.2035

$$f(x)=-\{\frac{Px^3}{6E_sI_{eq}}+\frac{P}{E_sI_{eq}}(\frac{b^2}{2}-a^2-al-lb)x+\frac{Pa^3}{3E_sI_{eq}}-\frac{Pa^3}{3E_sI_s}\} \quad a\le x\le b \tag{13b}$$

$$f(x)=-\{\frac{P(a+b)}{2E_sI_{eq}}x^2-\frac{P(a+b)(a+l)}{E_sI_{eq}}x+\frac{Pb^3}{6E_sI_{eq}}+\frac{Pab^2}{2E_sI_{eq}}+\frac{Pa^3}{3E_sI_{eq}}-\frac{Pa^3}{3E_sI_s}\} \quad b\le x\le a+l \tag{13c}$$

Substituting correlated parameters in Table 1 into Eq.(13), the deflection distribution of the CFRP reinforced beam can be figured out and displayed in Figure 5. It can be noted that the deflection shows a gradual increase from the end supports to the midspan of the beam. The slope of the deflection curve at the CFRP reinforced zone is smaller than that at the H-steel zone. The CFRP plate increases the flexural rigidity and enhances the deformation resistance of the steel beam.

To check the effect of the smart CFRP-FBG plate on the enhancement of bending rigidity of the steel beam, the comparison study on the deflections of the beam with and without CFRP plate is performed. Substituting E_SI_S to replace E_SI_{eq} in Eq.(13), the deflection of the steel beam without CFRP reinforcement can be calculated out, as shown in Figure 5. It can be noted that the CFRP plate can effectively enhance the bending rigidity of the beam.

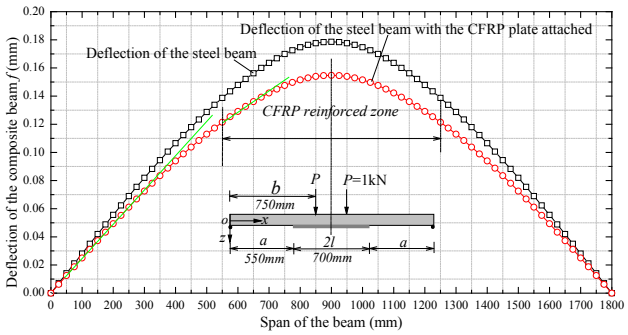

Figure 5. Deflection of the CFRP reinforced beam along with the span

4. Experimental Study

To check the accuracy of the proposed method for the deflection calculation, a smart CFRP-FBG composite reinforced steel beam has been designed, as shown in Figure 6. The length of the smart CFRP plate is 700 mm. The FBG sensor layout follows Ref. [14]. The span of the steel beam is 1800 mm, and the height and width are both 125 mm. The web width of the H-shaped cross section is 6 mm and the flange thickness is 9 mm. The four-point bending loading mode is designed and the distance between the two loading points is 300 mm. Seven LVDTs are installed to measure the deflections of the steel beam and the CFRP plate, as shown in Figure 6(a). The experimental set-up follows Figure 6(b).

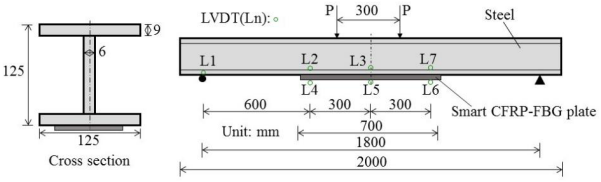

(a)

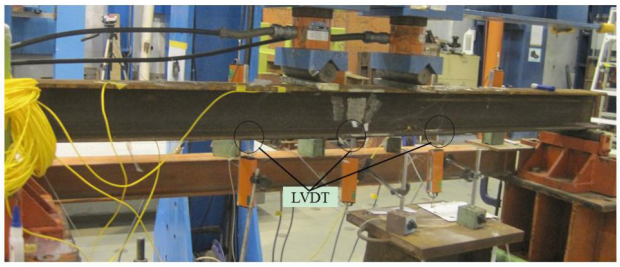

(b)

Figure 6. The experimental set-up of the smart CFRP-FBG reinforced beam

The deflections calculated by the proposed formula and the measured values are displayed in Figure 7. It can be noted that the calculated deflections are very close to the measured values of the smart CFRP reinforced beam under three different loads. The maximum error between the calculated deflection and the measured one is below 0.5 mm. The narrow gap between the two kinds of curves may be attributed to the ignorance of the self-weight of the reinforced beam in the proposed theoretical method, which leads to the measured deflections generally larger than the calculated values. In general, the proposed theoretical method can be used to much accurately describe the deflections of the CFRP reinforced beam. The influence of the parameters (i.e., length, strength and thickness) of the smart CFRP-FBG plate on the reinforcement effect will be carefully explored in further study.

The smart CFRP-FBG reinforced steel beam suffers from the plate end interfacial debonding when the load is up to 120 kN. The load-deflection curve of the beam at the mid span is displayed in Figure 8. The comparison of the mid-span deflections of the beams with and without CFRP composites by experimental study is also presented in Figure 8. It also proves that the CFRP plate can improve the bending rigidity of the beam.

Since the reinforced beam can suffer from different damage modes, the failure criterion of the smart CFRP-FBG reinforced steel beam will be carefully considered based on plenty of experimental study in future work.

DOI: https://doi.org/10.30564/jaeser.v3i4.2035

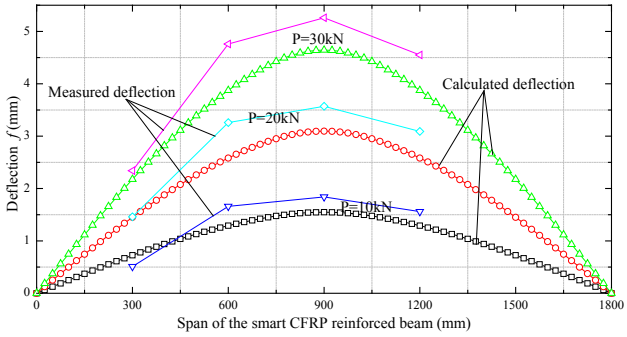

Figure 7. Deflections of the smart CFRP reinforced beam under different loads

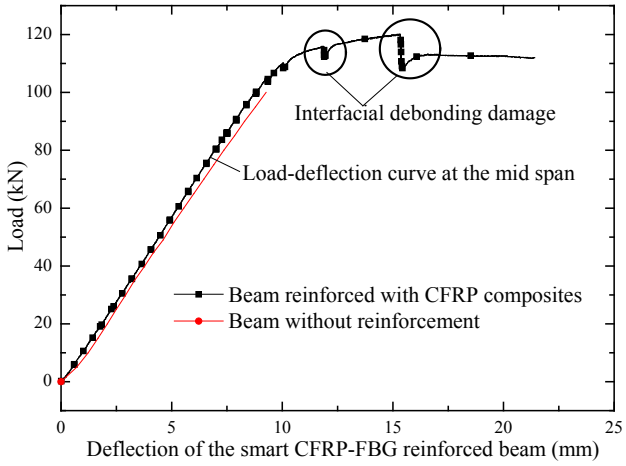

Figure 8. The load-deflection curve of the beam at the mid span

5. Conclusions

To understand the structural performance of CFRP reinforced beam structures, the stress state and the deflection of the composite beam has been discussed to explore the evolution principle. A theoretical method is proposed to calculate the deflection of the CFRP reinforced beam, and experimental tests are provided to validate the effectiveness of the derived formula. The following conclusions can be drawn from the study:

(1) The interfacial shear stress and the normal stress of the CFRP plate are both in direct proportion to the applied loads. The large value of interfacial shear stresses occurs in the end of the CFRP plate. The increase of loads on the beam can lead to the plate end interfacial debonding damage.

(2) The proposed theoretical method can be used to describe the deflection of the CFRP reinforced beam. Generally, the self-weight of the beam can be considered as a uniform line load applied to the beam, and the suggested formula (13) can be much accurately.

(3) The CFRP plate reinforced zone generally has larger bending rigidity than that of the pure steel beam zone, which means that the reinforced measure can efficiently improve the deformation resistance of the beam.

Acknowledgments

The work described in this paper was supported by the National Natural Science Foundation of China (Grant No. 51908263), Double First-Class (First-Class University & First-Class Disciplines) Funds of Lanzhou University (Grant No. 561119201), the Fundamental Research Funds for the Central Universities (Grant No. lzujbky-2020-56) and Key Laboratory of Structures Dynamic Behavior and Control (Ministry of Education) in Harbin Institute of Technology (Grant No. HITCE201901).

References

[1] Smith S.T., Teng J.G. Interfacial stresses in plated beams. Engineering Structures, 2001, 23, 857-871.

[2] Saadatmanesh H., Malek A.M. Design guidelines for flexural strengthening of RC beams with FRP plates. Journal of Composites for Construction, 1998, 2(4): 158-164.

[3] Jianguo Dai, Tamon Ueda, Yasuhiko Sato. Development of nonlinear bond stress-slip model of FRP sheet-concrete interfaces with a simple method[J]. Journal of Composites for Constructions, 2005, 9(1): 52-62.

[4] Gao W.Y., Dai J.G., Teng J.G. Analysis of mode II debonding behavior of fiber-reinforced polymer-to-substrate bonded joints subjected to combined thermal and mechanical Loading. Eng. Fract. Mech., 2015, 136: 241-264.

[5] Ceroni F., Ianniciello M., Pecce M. Bond behavior of FRP carbon plates externally bonded over steel and concrete elements: experimental outcomes and numerical investigations. Composites Part B: Engineering, 2016, 92: 434-446.

[6] Sikdar S., Mirgal P., Banerjee S., Ostachowicz W. Damage-induced acoustic emission source monitoring in a honeycomb sandwich composite structure. Composites Part B: Engineering, 2019, 158: 179-188.

[7] Filippo Bastianini, Marco Corradi, Antonio Borri, Angelo di Tommaso. Retrofit and monitoring of an historical building using “Smart” CFRP with embedded fibre optic Brillouin sensors. Construction and Building Materials, 2005, 19: 525-535.

[8] Takeda S., Okabe Y., Yamamoto T., Takeda N. Detection of edge delamination in CFRP laminates under cyclic loading using small-diameter FBG sensors. Composites Science and Technology, 2003, 63: 1885-

DOI: https://doi.org/10.30564/jaeser.v3i4.2035

1894.

[9] Mizutani T., Okabe Y., Takeda N. Quantitative evaluation of transverse cracks in carbon fiber reinforced plastic quasi-isotropic laminates with embedded small-diameter fiber Bragg grating sensors. Smart Materials and Structures, 2003, 12: 898-903.

[10] Huaping Wang, Ping Xiang, Lizhong Jiang. Strain transfer theory of industrialized optical fiber-based sensors in civil engineering: a review on measurement accuracy, design and calibration. Sensors & Actuators A: Physical, 2019, 285: 414-426.

[11] Takeda S., Aoki Y., Nagao Y. Damage monitoring of CFRP stiffened panels under compressive load using FBG sensors. Composite Structures, 2012, 94: 813-819.

[12] Lammmens N., Luyckx G., Voet E., Paepegem W. V., Degrieck J. Optimization of coating diameter of fiber optic sensors embedded in composite structures under arbitrary loading conditions. Smart Materials and Structures, 2015, 24: 115003-1-12.

[13] Huaping Wang, Jianguo Dai. Strain transfer analysis of fiber Bragg grating sensor assembled composite structures subjected to thermal loading. Composites Part B: Engineering, 2019, 162: 303-313.

[14] Huaping Wang, Yiqing Ni, Jianguo Dai, Maodan Yuan. Interfacial debonding detection of strengthened steel structures by using smart CFRP-FBG composites[J]. Smart Materials and Structures, 2019, 28-115001-1-13.

[15] Taljsten B. Strengthening of beams by plate bonding. Journal of Materials and Civil Engineering, 1997, 9(4): 206-212.

 DOI: https://doi.org/10.30564/jaeser.v3i4.2035